A quasiclassical analysis of second-harmonic generation

1995 J. Phys. A: Math. Gen. 28 3439

(http://iopscience.iop.org/0305-4470/28/12/017)

J. Phys. A: Math. Gen. 28 (1995) 3439–3451. Printed in the UK

A quasiclassical analysis of second-harmonic generation

R F Alvarez-Estrada†, A Gómez Nicola†, L L Sánchez-Soto‡ and A Luis‡

† Departamento de Física Teórica I, Facultad de Ciencias Físicas, Universidad Complutense, 28040 Madrid, Spain

‡ Departamento de Optica, Facultad de Ciencias Físicas, Universidad Complutense, 28040 Madrid, Spain

Received 8 November 1994, in final form 28 March 1995

Abstract. We investigate a quantum two-oscillator model for second-harmonic generation. The total Hamiltonian is the sum of two commuting Hamiltonians with eigenvalues E_0 and $E_{\rm int}$. The exact determination of these eigenvalues is studied using tridiagonal matrices. We present two general equations in the quasiclassical regime yielding the largest $E_{\rm int}$ for a given E_0 and a representation for both eigenvalues in terms of an additional quantum number. Some numerical analysis shows that both equations are fairly consistent for suitably large quantum numbers with the exact quantum results. An approximate analytical expression for the wavefunction is also given.

1. Introduction

Second-harmonic generation is perhaps the simplest nonlinear optical process. Classically, it corresponds to the generation of a field at frequency 2ω (second-harmonic mode) when an intense pump field of frequency ω (fundamental mode) propagates in a nonlinear medium. This problem can be handled in a closed analytical way describing the possibility of complete energy transfer into the second-harmonic mode [1, 2].

For quantum fields, this process can be envisioned as two identical photons of frequency ω coalescing within the medium to form a single photon of frequency 2ω, which can be described by the effective Hamiltonian

$$H = \hbar\omega a^\dagger a + 2\hbar\omega b^\dagger b + \hbar g\left(b^\dagger a^2 + b a^{\dagger 2}\right) \tag{1.1}$$

where a and b are the annihilation operators of the fundamental and second-harmonic mode, respectively, and the constant g describes the coupling between modes.

Unfortunately for this quantum Hamiltonian the dynamics is a touchy business. Exact solutions were given recently in the framework of the algebraic Bethe ansatz [3], but direct application of them to the problem at hand seems rather difficult [4]. The parametric approximation in which the pump depletion is neglected (i.e. it is treated as a classical field of constant amplitude) is often used [5–8], as well as numerical approximations [9–11]. Irrespective of the approach chosen, the quantum fluctuations prevent the complete transfer of energy into the second harmonic and the solutions become oscillatory. Moreover, this model can exhibit a rich spectrum of non-classical features such as photon antibunching [12], squeezing [13, 14], or collapses and revivals [15]. In fact, it has recently been found that the fundamental mode evolves into a superposition of macroscopically distinguishable states or *cat* states [16–18].

0305-4470/95/123439+13$19.50

The aim of the present paper is to study some asymptotic behaviours of the dynamics described by the Hamiltonian (1.1). The spectrum of the interaction part of the Hamiltonian is analysed numerically and an asymptotic formula for the largest eigenvalue, when the number of photons is high enough, is obtained. The numerical eigenvalues are used to study the time evolution of the second-harmonic mode, which displays a physically interesting behaviour: a kind of collapse–revival phenomenon. We employ the quasiclassical quantization rules to confirm the rich dynamical features of the model. Specifically, these rules yield an analytic representation, via elliptic functions, for the spectrum of the interaction Hamiltonian. The consistency of such a representation with the numerical analysis and with the asymptotic formula for the largest eigenvalue is fully established.

We believe that the various formulae mentioned above for the spectrum of the Hamiltonian may be of great utility in further analysis of second-order phenomena.

2. Quantum dynamics of the second-harmonic generation

As we have mentioned, second-harmonic generation is described by the Hamiltonian

$$H = H_0 + H_{\rm int} \tag{2.1}$$

with

$$H_0 = \hbar\omega a^\dagger a + 2\hbar\omega b^\dagger b \qquad H_{\rm int} = \hbar g\left(b^\dagger a^2 + b a^{\dagger 2}\right). \tag{2.2}$$

By using the standard bosonic commutation relations ($[a, a^\dagger] = I$, $[b, b^\dagger] = I$, $[a, b] = 0$) it is straightforward to check that

$$\begin{aligned}[H_0, H_{\rm int}] &= \hbar^2\omega g\left[a^\dagger a + 2b^\dagger b,\, b^\dagger a^2 + b a^{\dagger 2}\right] \\ &= \hbar^2\omega g\left(-2a^2 b^\dagger + 2a^2 b^\dagger + 2b a^{\dagger 2} - 2b a^{\dagger 2}\right) = 0\end{aligned} \tag{2.3}$$

so, both are constants of motion. This allows us to factor out $\exp(-{\rm i}H_0 t/\hbar)$ from the evolution operator and drop it. The common eigenstates of H_0 and $H_{\rm int}$, with eigenvalues $E_0 = \hbar\omega N$ and $E_{\rm int} = \hbar g\Lambda$, respectively, are characterized through

$$|N, \Lambda\rangle' = \sum_{\substack{n_a, n_b \\ n_a + 2n_b = N}} \langle n_a, n_b | N, \Lambda\rangle' \, |n_a, n_b\rangle \tag{2.4}$$

with

$$|n_a, n_b\rangle = \frac{b^{\dagger n_b} a^{\dagger n_a}}{\sqrt{n_a! n_b!}} |0, 0\rangle \tag{2.5}$$

where $|0, 0\rangle$ is the vacuum state for both modes and $n_a, n_b = 0, 1, \ldots$. In this Fock basis, $H_{\rm int}$ is non-diagonal. However, since $n_a + 2n_b = N =$ constant, H_0 splits the field space into orthogonal spaces that have $[N/2] + 1$ components, where $[N/2]$ means the integer part of $N/2$. Thus, for a given N we can relabel the states (2.5) as

$$|n_a, n_b\rangle \equiv |N - 2k, k\rangle \tag{2.6}$$

which form a complete set, and $H_{\rm int}$ is represented in this latter basis by the tridiagonal matrix of order $([N/2] + 1) \times ([N/2] + 1)$ [19]

$$H_{\rm int} = \hbar g \begin{pmatrix} 0 & c_0 & 0 & \ldots & \ldots \\ c_0 & 0 & c_1 & 0 & \ldots \\ 0 & c_1 & 0 & c_2 & \ldots \\ \vdots & \vdots & \vdots & \ddots & \end{pmatrix} \tag{2.7}$$

where

$$c_k = \sqrt{(k+1)(N-2k)(N-2k-1)}\,. \tag{2.8}$$

It is easy to check that due to the properties of tridiagonal matrices, the eigenvalues Λ are distributed symmetrically with respect to zero, with one eigenvalue equal to zero if there are an odd number of them.

The adoption of the Fock number-state basis does not accord well with a realistic representation of coherent laser light. Later we shall work with coherent states, that are expressed as number state superpositions. However, to start with let us assume that at $t = 0$ the system is in the state $|N, 0\rangle$. To find the state evolution, we need the matrix elements of the evolution operator

$$C_{N,k}(t) = \langle N-2k, k|\exp(-\mathrm{i}H_{\mathrm{int}}t/\hbar)|N, 0\rangle \tag{2.9}$$

which can be written as

$$C_{N,k}(t) = \sum_{i=0}^{[N/2]} \mathrm{e}^{-\mathrm{i}g t\Lambda_i} U_{k,i} U^*_{0,i} \tag{2.10}$$

where $\Lambda_i = \Lambda_0, \ldots, \Lambda_{[N/2]}$ are the eigenvalues and U is the unitary matrix that diagonalizes the interaction Hamiltonian matrix. If the eigenvalues are sorted from the lowest to the highest values, we have the symmetry relation [19]

$$U_{k,i}U_{0,i} = (-1)^k U_{k,[N/2]-i}U_{0,[N/2]-i} \tag{2.11}$$

which makes the coefficients $C_{N,k}$ real when k is even and imaginary when k is odd.

Many authors have carried out the diagonalization of H_{int} numerically. However, we wish to draw attention to one important point which does not seem to have been stated in previous works on the subject: the largest possible eigenvalue of H_{int} for a fixed N follows a power law of the form (when N is high enough)

$$\Lambda_{\max} \approx \frac{4}{3\sqrt{6}} N^{3/2}\,. \tag{2.12}$$

This has been carefully checked in all our numerical computations and can be recovered by a simple argument as follows: for $N \gg 1$, the dominant contributions can be expected to correspond to large values of both n_a and n_b. Then both modes may be expected to be close to the classical limit in which the associated operators a and b may be approximately replaced by classical c-numbers α and β, in such a way that

$$N \approx \alpha^2 + 2\beta^2 \qquad \Lambda \approx 2\alpha^2\beta\,. \tag{2.13}$$

Then

$$\Lambda \approx 2(N - 2\beta^2)\beta\,. \tag{2.14}$$

For a fixed N, the maximum eigenvalue occurs when $\mathrm{d}\Lambda/\mathrm{d}\beta = 0$, which immediately gives

$$\alpha = 2(N/6)^{1/2} \qquad \beta = (N/6)^{1/2} \tag{2.15}$$

from which the power law (2.12) follows. In numerical computations this scaling law works quite accurately even when $N \approx 10$ (see table 1).

The important scaling law (2.12) will be confirmed again, in a different setting, in (3.11), and it will play an essential role in the analysis of the quasiclassical quantization rules and the discussion about them.

Table 1. Comparison between the exact maximum eigenvalue of $H_{\rm int}$ for fixed n and the bound obtained using (2.19).

N	$\Lambda_{\max}^{(\rm exact)}$	$\Lambda_{\max}^{(\rm approx)}$	Relative error %
10	16.613	17.213	3.61
20	47.838	48.686	1.77
30	88.404	89.442	1.17
40	136.507	137.706	0.88
50	191.109	192.450	0.88
60	251.513	252.982	0.58
70	317.208	318.794	0.50
80	387.796	389.491	0.44
90	462.959	464.758	0.39
100	542.438	544.331	0.35

The typical conditions for second-harmonic generation are a coherent state for the fundamental mode and the vacuum for the second-harmonic mode. Thus, we suppose the initial state of the form

$$|\psi(0)\rangle = \sum_{N=0}^{\infty} b_N |N, 0\rangle \tag{2.16}$$

where

$$b_N = \mathrm{e}^{-|\alpha|^2/2} \frac{\alpha^N}{\sqrt{N!}} \tag{2.17}$$

is the Poissonian weighting factor of the coherent state $|\alpha\rangle$ and $|\alpha|^2$ is the mean photon number. With this initial condition the resulting state is

$$|\psi(t)\rangle = \sum_{N=0}^{\infty} b_N \sum_{k=0}^{[N/2]} C_{N,k}(t) |N-2k, k\rangle \tag{2.18}$$

with $C_{N,k}(t)$ given by (2.10). This series has been evaluated numerically in a number of papers showing a clear oscillatory behaviour that decays faster for higher n_a, so here we do not intend to give an extensive discussion of this problem. Rather, we wish to give an approximate analytic expression for the wavefunction. To this end, let us now expand in (2.16) the state $|N, 0\rangle$ in the basis $|N, \Lambda\rangle'$ of eigenstates of $H_{\rm int}$

$$|N, 0\rangle = \sum_{j=0}^{[N/2]} a_{j,N} |N, \Lambda_j\rangle' . \tag{2.19}$$

The distribution probabilities $|a_{j,N}|^2$, which indicate the overlap between the state $|N, 0\rangle$ and the eigenstates $|N, \Lambda_j\rangle'$, can be studied numerically. The central point, as discussed in detail in [15], is that for N high enough and $N = 2k$ (even) this decomposition can be well approximated by considering only three eigenstates: zero and two of them (Λ_1 and $-\Lambda_1$) distributed symmetrically with respect to zero and of maximum overlap, obtaining

$$|\psi_{2k}(0)\rangle = |2k, 0\rangle \approx a_{0,2k} |2k, 0\rangle' + a_{1,2k} |2k, \Lambda_1\rangle' + a_{1,2k} |2k, -\Lambda_1\rangle' \tag{2.20}$$

where the coefficients of $|2k, \Lambda_1\rangle'$ and $|2k, -\Lambda_1\rangle'$ are the same by symmetry. The time evolution of this state is

$$|\psi_{2k}(t)\rangle = a_{0,2k} |2k, 0\rangle' + a_{1,2k} \mathrm{e}^{-\mathrm{i}g\Lambda_1 t} |2k, \Lambda_1\rangle' + a_{1,2k} \mathrm{e}^{\mathrm{i}g\Lambda_1 t} |2k, -\Lambda_1\rangle' . \tag{2.21}$$

Analogously, when $N = 2k + 1$ (odd) we can accurately approximate the expansion by the two symmetric eigenvalues (Λ_2 and $-\Lambda_2$) of maximum overlap

$$|\psi_{2k+1}(0)\rangle = |2k+1,0\rangle \approx a_{2,2k+1}|2k+1,\Lambda_2\rangle' + a_{2,2k+1}|2k+1,-\Lambda_2\rangle' \tag{2.22}$$

with a time evolution

$$|\psi_{2k+1}(t)\rangle = a_{2,2k+1}\,\mathrm{e}^{-\mathrm{i}g\Lambda_2 t}|2k+1,\Lambda_2\rangle' + a_{2,2k+1}\,\mathrm{e}^{\mathrm{i}g\Lambda_2 t}|2k+1,-\Lambda_2\rangle'. \tag{2.23}$$

The time evolution of the system is

$$|\psi(t) = \sum_{k=0}^{\infty} b_{2k}|\psi_{2k}(t)\rangle + \sum_{k=0}^{\infty} b_{2k+1}|\psi_{2k+1}(t)\rangle. \tag{2.24}$$

We can now give an approximate expression for the evolution of the second-harmonic field as

$$\begin{aligned}\langle n_b\rangle = \sum_{k=0}^{\infty} b_{2k}^2\big[&2a_{0,2k}a'_{1,2k}\langle 2k,0|b^\dagger b|2k,\Lambda_1\rangle'\cos(g\Lambda_1 t)\\ &+2a_{0,2k}a'_{1,2k}\langle 2k,0|b^\dagger b|2k,-\Lambda_1\rangle'\cos(g\Lambda_1 t)\\ &+2a'^2_{1,2k}\langle 2k,\Lambda_1|b^\dagger b|2k,-\Lambda_1\rangle'\cos(2g\Lambda_1 t) + a'^2_{0,2k}\langle 2k,0|b^\dagger b|2k,0\rangle'\\ &+a'^2_{1,2k}\langle 2k,\Lambda_1|b^\dagger b|2k,\Lambda_1\rangle' + a'^2_{1,2k}\langle 2k,-\Lambda_1|b^\dagger b|2k,-\Lambda_1\rangle'\big]\\ &+\sum_{k=0}^{\infty} b_{2k+1}^2\big[2a'^2_{2,2k+1}\langle 2k+1,\Lambda_2|b^\dagger b|2k+1,-\Lambda_2\rangle\cos(2g\Lambda_2 t)\\ &+a'^2_{2,2k+1}\langle 2k+1,\Lambda_2|b^\dagger b|2k+1,\Lambda_2\rangle'\\ &+a'^2_{2,2k+1}\langle 2k+1,-\Lambda_2|b^\dagger b|2k+1,-\Lambda_2\rangle'\big].\end{aligned} \tag{2.25}$$

Here the time evolution is proportional to the cosines of $g\Lambda_1 t$, $2g\Lambda_1 t$ and $g\Lambda_2 t$. The presence of these different frequencies implies the impossibility of monotonic growth of the intenstity as in the classical case, and clearly shows the oscillatory character of the quantum solution, interference among these components appears to be responsible for these oscillations.

Moreover, the existence of small oscillations around some stationary value has been observed numerically for large times with significant decreases and oscillations at particular times, showing a kind of collapse–revival behaviour. The explanation of this behaviour is now straightforward by means of similar arguments to those for the Jaynes–Cummings model [20]. Using the actual values of the eigenvalues, we have plotted the evolution of the second-harmonic mode in figure 1, finding very good agreement with the numerical computations.

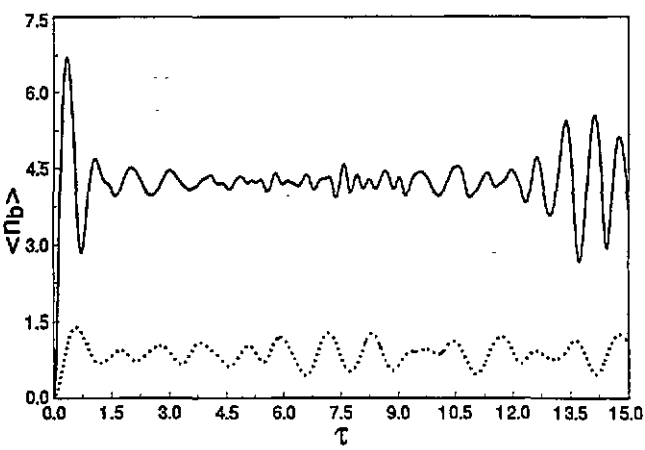

Figure 1. Plots of the mean photon number in the second-harmonic mode versus $\tau = gt$, for $n_a = 4$ (broken curve) and $n_a = 16$ (full curve). In both cases we have used the approximation (2.25).

3. Quasiclassical evolution of the second-harmonic mode

3.1. Canonical variables

We shall introduce the Hermitian operators x_j, $p_j (j = 1, 2)$ through

$$a = \sqrt{\frac{\omega}{2\hbar}} x_1 + \frac{\mathrm{i}}{\sqrt{2\hbar\omega}} p_1 \qquad b = \sqrt{\frac{\omega}{\hbar}} x_2 + \frac{\mathrm{i}}{2\sqrt{\hbar\omega}} p_2 \tag{3.1}$$

and so on for $a^\dagger$ and $b^\dagger$. One has $[x_j, p_j] = \mathrm{i}\hbar$ and all other commutators vanish. We can always set $p_j = -\mathrm{i}\hbar\partial/\partial x_j$. Note that there is no compelling reason to treat x_j as position operators for photons in ordinary space. Rather, x_j and p_j should be identified as proportional to the amplitudes of the two quadrature phases of the electric field, which may be measured experimentally by means of optical homodyne detection [21].

In order to approach the classical limit $\hbar \to 0$ properly, we shall introduce a new coupling constant f defined by

$$\hbar g = -\sqrt{2}\hbar^{3/2} f \,. \tag{3.2}$$

By substituting in the Hamiltonian of the system one gets

$$\begin{aligned} H_0 &= \frac{p_1^2}{2} + \frac{\omega^2}{2} x_1^2 + \frac{p_2^2}{2} + \frac{(2\omega)^2}{2} x_2^2 - \frac{3}{2}\hbar\omega \\ H_{\mathrm{int}} &= -f\left[(2\omega)^{1/2}(\omega x_1^2 - \omega^{-1} p_1^2) x_2 + (2\omega)^{-1/2}(x_1 p_1 + p_1 x_1) p_2\right]. \end{aligned} \tag{3.3}$$

We shall consider the classical limit of this quantized model. Then, the operators x_j and p_j become classical (c numbers) commuting variables we shall denote by x_j and $p_{j,c}$. Consequently the operators in (3.3) become the classical Hamiltonians

$$\begin{aligned} H_{0,\mathrm{c}} &= \frac{p_{1,\mathrm{c}}^2}{2} + \frac{\omega^2}{2} x_1^2 + \frac{p_{2,\mathrm{c}}^2}{2} + \frac{(2\omega)^2}{2} x_2^2 \\ H_{\mathrm{int,c}} &= -f\left[(2\omega)^{1/2}(\omega x_1^2 - \omega^{-1} p_{1,\mathrm{c}}^2) x_2 + (2\omega)^{-1/2} 2 x_1 p_{1,\mathrm{c}} p_{2,\mathrm{c}}\right] \end{aligned} \tag{3.4}$$

respectively. One can easily check that the classical Poisson bracket of $H_{0,\mathrm{c}}$ and $H_{\mathrm{int,c}}$ vanishes.

We shall obtain some approximate analytical representations for the eigenvalues $E_{0,\mathrm{c}}$ and $E_{\mathrm{int,c}}$ in the quasiclassical limit (the subscript c will remind that one is calculating only in this limit). In so doing, use will be made of the generalization of the Bohr–Sommerfeld quantization rules due to Einstein [22], Brillouin [23] and Keller [24]. We shall limit ourselves to giving the quasiclassical representations which yield $E_{0,\mathrm{c}}$ and $E_{\mathrm{int,c}}$ implicitly, and to study numerically their consistency with the results of the exact quantum analysis. This quasiclassical analysis has its own interest, as it is a highly non-trivial application of the quantization rules and may be useful for further studies of the system at hand.

3.2. Classical solutions for momenta and their structure

We start by setting

$$H_{0,\mathrm{c}} = E_{0,\mathrm{c}} \qquad H_{\mathrm{int,c}} = E_{\mathrm{int,c}} \,. \tag{3.5}$$

Equations (3.5) constitute a system that enables to determine $p_{1,c}$ and $p_{2,c}$ in terms of x_1 and x_2. Notice that $p_{1,c}$ is obtained by solving a quartic equation. One finds

$$p_{1,c}(\sigma,\rho)=\sigma\left[\frac{C_0+\rho\Delta^{1/2}x_1^2}{2(x_1^2+x_2^2)}\right]^{1/2}$$
$$p_{2,c}(\sigma,\rho)=\frac{(2\omega)^{1/2}}{2fx_1p_{1,c}(\sigma,\rho)}\left[\frac{fx_2(2\omega)^{1/2}}{\omega}p_{1,c}^2(\sigma,\rho)-B_2\right] \tag{3.6}$$

where $\sigma=\pm$, $\rho=\pm$, and

$$C_0=B_1x_1^2+B_2f^{-1}(2\omega)^{1/2}x_2 \qquad \Delta=C_+C_-$$
$$C_\pm=B_1+\frac{x_2(2\omega)^{1/2}}{fx_1^2}B_2\pm\frac{(2\omega)^{1/2}}{fx_1}\left[1+\left(\frac{x_2}{x_1}\right)^2\right]^{1/2}B_2 \tag{3.7}$$
$$B_1=2E_{0,c}-\omega^2x_1^2-(2\omega)^2x_2^2 \qquad B_2=E_{\mathrm{int},c}+f\omega(2\omega)^{1/2}x_1^2x_2\,.$$

For a given $E_{0,c}>0$, a necessary condition for the existence of allowed classical trajectories is $B_1\geqslant 0$ for any x_1, x_2, as (3.5) and (3.7) show. Notice that $B_1=0$ (which represents an ellipse in the (x_1,x_2) plane) implies that $p_{1,c}(\sigma,\rho)=p_{2,c}(\sigma,\rho)=0$ and, for the sake of consistency, $B_2=0$ also.

For classical trajectories to exist at (x_1,x_2) $p_{1,c}^2$ should be real and non-negative and $p_{1,c}^2<B_1$. No further conditions on $p_{2,c}$ are required.

For a given $E_{0,c}(>0)$ and a suitable $E_{\mathrm{int},c}(<0)$, figure 2 displays in the (x_1,x_2)-plane:

(i) The region $B_1>0$ (that is, the interior of the ellipse $B_1=0$).
(ii) The curves $C_+=0$ and $C_-=0$.
(iii) The curve $B_2=0$.

Except for some specific features, the detailed form of those curves is not very relevant. Each one of the curves (ii) and (iii) is always symmetric about the x_2-axis. The interest in curve (iii) will be appreciated soon.

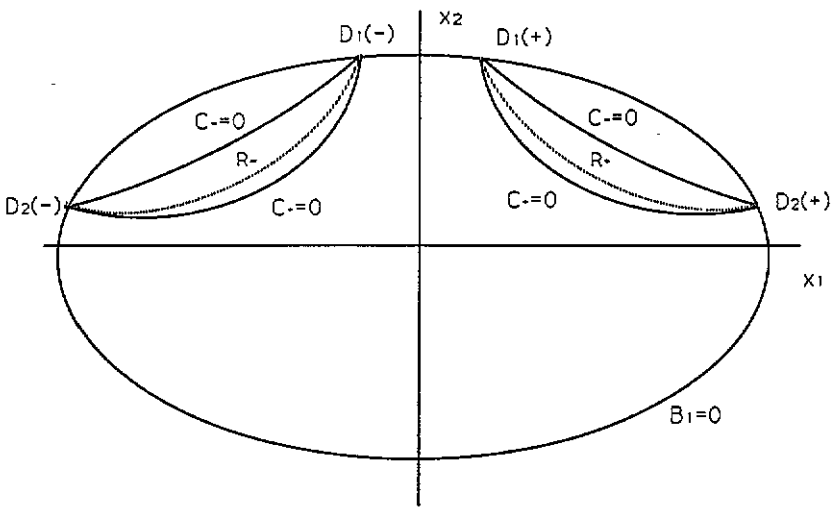

Figure 2. The classically allowed regions R_+, R_- are limited by the curves $C_-=0$ and $C_+=0$. The curve $B_2=0$ (indicated in the figure as dotted) always lies below $C_-=0$ and above $C_+=0$ and it intersects the ellipse $B_1=0$ at the points $D_1(+)$, $D_2(+)$ (right branch) and $D_1(-)$ and $D_2(-)$ (left branch).

The solutions of the system

$$B_1 = 0 \qquad B_2 = 0 \tag{3.8}$$

correspond to the four points $D_1(+)$, $D_2(+)$, $D_1(-)$ and $D_2(-)$ in figure 2. The system (3.8) yields

$$x_2^3 - \frac{E_{0,c}}{2\omega^2} x_2 - \frac{E_{int,c}}{4f\omega(2\omega)^{1/2}} = 0 . \tag{3.9}$$

A study of the explicit solutions of (3.9) is now in order. The main conclusions may be summarized as follows.

First, the intersections of $B_1 = 0$ and $B_2 = 0$ give rise to four different points (as in figure 2) only if

$$E_{int,c}^2 < \frac{16}{27}\frac{f^2}{\omega^3} E_{0,c}^3 . \tag{3.10}$$

The points $D_1(+)$ and $D_2(+)$ coincide with each other (as do the symmetric points $D_1(-)$ and $D_2(-)$ with each other) when

$$E_{int,c}^2 = \frac{16}{27}\frac{f^2}{\omega^3} E_{0,c}^3 \tag{3.11}$$

and, in this case, the double solution of (3.9) yields for $D_1(+)$ and $D_2(+)$

$$x_2 = -\frac{1}{2}\left[\frac{E_{int,c}}{f\omega(2\omega)^{1/2}}\right]^{1/3} > 0 . \tag{3.12}$$

The system (3.8) has no acceptable solution if $E_{int,c}^2 > \frac{16}{27}\frac{f^2}{\omega^3} E_{0,c}^3$. In such a case, the intersection of the ellipse $B_1 = 0$ and the curve $B_2 = 0$ is empty.

For $E_{int,c}$ fulfilling (3.10), the allowed classical trajectories correspond to points inside the regions R_+, R_- limited by $C_+ = 0$ and $C_- = 0$, where $\Delta \geqslant 0$. Note that R_+ is obtained through reflection symmetry from R_- with respect to the x_2-axis.

An important point is that the condition (3.11) coincides precisely with the scaling law (2.12) when one uses $E_{0,c} = \hbar\omega N$ and $E_{int,c} = -2^{1/2}\hbar^{3/2} f \Lambda_{max}$.

We shall now concentrate on the (x_1, x_2)-plane and, in particular, on the domain R_+ (with $x_1 > 0$) inside of which $\Delta > 0$ (with $E_{int,c} < 0$, which is not an essential restriction). Then, we consider three additional copies of them. Altogether, they define a four-sheeted (x_1, x_2) space (the so called covering space [24]). We shall use (σ, ρ) and $p_{1,c}(\sigma, \rho)$ to characterize and distinguish these sheets. We shall denote by $C_-(\sigma, \rho) = 0$ and $C_+(\sigma, \rho) = 0$ the curves in the sheet (σ, ρ) along which $\Delta = 0$, and by $R_+(\sigma, \rho)$ the domain which is enclosed by these two curves.

A careful study of $p_{1,c}(\sigma, \rho)$ and $p_{2,c}(\sigma, \rho)$ in the various sheets has been undertaken in order to connect the latter among themselves whenever possible in such a way that these functions vary in a continuous way. In other words, these functions become univalued in the covering space. The results of such an analysis are the following:

(i) The two domains $R_+(+,+)$ and $R_+(+,-)$ can be joined across $C_-(+,+) = 0$, $C_-(+,-) = 0$ and across $C_+(+,+) = 0$, $C_+(+,-) = 0$. The union of $R_+(+,+)$ and $R_+(+,-)$ will be named $R_+(+)$.

(ii) The same holds true for the domain $R_+(-,+)$ and $R_+(-,-)$ across $C_-(-,+) = 0$, $C_-(-,-) = 0$ and across $C_+(-,+) = 0$, $C_+(-,-) = 0$. The union of $R_+(-,+)$ and $R_+(-,-)$ will be denoted by $R_+(-)$. Both $R_+(+)$ and $R_+(-)$ are displayed in figure 3(*a*).

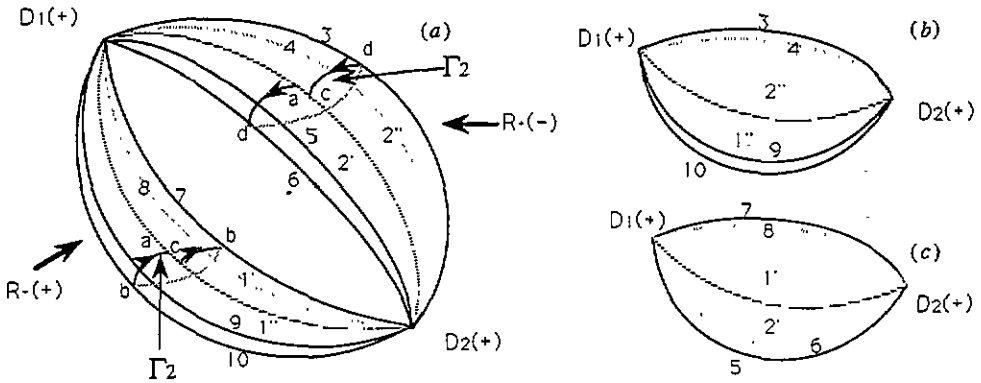

Figure 3. (*a*) The regions $R_+(-)$ (upper) and $R_+(+)$ (lower) are displayed. The notation for the different curves is as follows: 3: $C_+(-,-)=0$; 4: $C_+(-,+)=0$; 5: $C_-(-,-)=0$; 6: $C_-(-,+)=0$; 7: $C_-(+,-)=0$; 8: $C_-(+,+)=0$; 9: $C_+(+,-)=0$; 10: $C_+(+,+)=0$. The connections between $R_+(+)$ and $R_+(-)$ across the curves $B_2=0$ (indicated as dotted and unnumbered) are also given. The closed curve Γ_2 is also displayed. The symbols a, b, c, d indicate how the various parts of Γ_2 are connected to one another. (*b*) and (*c*) display the topological structure of the covering space $R_+(+)\cup R_+(-)$. $R_+(+)$ and $R_+(-)$ are joined across $B_2=0$ (also drawn as dotted and unnumbered) as indicated in the main text. Notice that $1''$ is not continuously connected to $2''$ neither is $1'$ to $2'$.

(iii) $R_+(+)$ and $R_+(-)$ are continuously connected (and, hence joined) to each other across the curves $B_2=0$ in $R_+(+,-)$ and $B_2=0$ in $R_+(-,-)$ (in both of which $p_{1,c}=0$). Specifically, the regions $1''$ and $2'$ of sheets $\sigma=-\rho=+$ and $\sigma=\rho=-$, respectively, should be joined to each other, and similarly, the regions $1'$ and $2''$ of sheets $\sigma=-\rho=+$ and $\sigma=\rho=-$, respectively, should be continuously connected to each other (see figure 3(*a*)). In this way, $p_{2,c}$ is guaranteed to vary continuously whenever $p_{1,c}$ vanishes.

We call $R_+(+)\cup R_+(-)$ the union of both $R_+(+)$ and $R_+(-)$ across the curve $B_2=0$. Its topological structure is shown in figures 3(*b*) and (*c*). The four-sheeted (x_1, x_2) space with connections among the various sheets is the covering space for carrying out the semiclassical quantization of the system, which we shall investigate in the next section.

We emphasize that the various connections among different sheets as displayed in figure 3 are dictated by Keller's general prescription. We also stress that the developments of this subsection are technically unavoidable in order to properly formulate the quasiclassical quantization rules.

3.3. Quasiclassical quantization rules

Let Γ_j $(j=1,2)$ be two suitable closed and topologically independent paths (that is, none of them can be continuously deformed so as to coincide with the other one) in $R_+(+)\cup R_+(-)$. A typical choice for Γ_2 and Γ_1 is displayed through figures 3(*a*) and 4. It will be assumed that Γ_2 cannot be infinitesimally close to $D_1(+)$ or $D_1(-)$. Such closed curves are described by the equations $\gamma_j(x_1, x_2)=0$.

We are now ready to apply the quantization rules in order to provide the implicit quasiclassical analytical formulae for $E_{0,c}$ and $E_{\mathrm{int},c}$, as announced before.

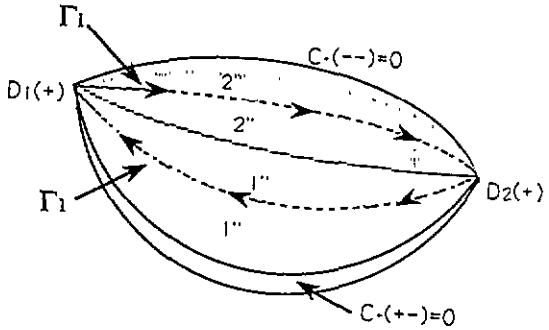

Figure 4. The closed curve Γ_1 is displayed using the same notation as in figure 3(*a*). Notice that for simplicity curves 4 and 8 are omitted. Γ_1 passes by both $D_1(+)$ and $D_2(+)$. A part of Γ_1 lies in the region $1''$ in the sheet $\sigma = -\rho = +$ (where $p_{2,c} > 0$), while the other part is contained in region $2''$ of sheet $\sigma = \rho = -$ (where $p_{2,c} < 0$)..

The quantization rules read as

$$\oint_{\Gamma_j} \left(p_{1,c}\,dx_1 + p_{2,c}\,dx_2\right) = 2\pi\hbar\left(n_j + \frac{\mu_j}{4}\right) \tag{3.13}$$

where $p_{1,c}$ and $p_{2,c}$ are given through (3.6) and the integrations extend along the whole closed paths Γ_j. In turn, n_j are arbitrary positive integers and μ_j are fixed integers called Maslov indices (or, more generally, Berry phases).

It is particularly convenient to choose Γ_1 so that $\gamma_1(x_1, x_2) = 0$ is precisely $B_2 = 0$. Equations (3.6) then imply that $p_{1,c} = 0$ along Γ_1, while $p_{2,c} = \pm B_1^{1/2}$ in the parts of Γ_1 lying in $1'', 2''$, respectively.

By using $y = x_1^2$ as integration variable, the left-hand side of (3.13) for $j = 1$ becomes an elliptic integral over y ($E_{\text{int,c}} < 0$):

$$\int_{y^{(1)}}^{y^{(2)}} \frac{dy}{y^3}\left[E_{0,c}y^2 - \frac{\omega^2}{2}y^3 - \frac{E_{\text{int,c}}^2}{f^2\omega}\right]^{1/2} = \frac{\omega^{3/2}f\pi}{-E_{\text{int,c}}}\hbar\left(n_1 + \frac{\mu_1}{4}\right) \tag{3.14}$$

where

$$y^{(h)} = -\frac{E_{\text{int,c}}}{f\omega(2\omega)^{1/2}x_2^{(h)}} \tag{3.15}$$

with $x_2^{(h)}$ the two positive solutions of (3.9) which corresponds to $D_h(+)$, $h = 1, 2$. Notice that $x_2^{(1)} > x_2^{(2)}$, so that $y^{(2)} > y^{(1)}$.

We argue that $\mu_1 = 0$ in (3.14). In fact, when (3.11) holds, one finds that

$$y^{(1)} = y^{(2)} = 2\left[-\frac{E_{\text{int,c}}}{f\omega(2\omega)^{1/2}}\right]^{2/3} \tag{3.16}$$

and, moreover, that the square root in the integrand of the left-hand side of (3.14) vanishes. For consistency, the right-hand side of (3.14) requires $n_1 = 0$ and hence $\mu_1 = 0$. When (3.10) holds, (3.14) is valid for a finite set of non-negative values for the integer n_1 (with $\mu_1 = 0$).

We introduce the dimensionless variables z, e, and u through

$$x_2 = \frac{\sqrt{E_{0,c}}}{\omega}z \qquad y = \frac{E_{0,c}}{\omega^2}u \qquad e = \frac{E_{\text{int,c}}\omega^{3/2}}{fE_{0,c}^{3/2}}. \tag{3.17}$$

Then, equations (3.14), (3.15) and (3.9) become, respectively,

$$n_1 = \frac{-eN}{\pi}\int_{u^{(1)}}^{u^{(2)}} \frac{du}{u^3}\left(u^2 - \frac{u^3}{2} - e^2\right)^{1/2} \tag{3.18a}$$

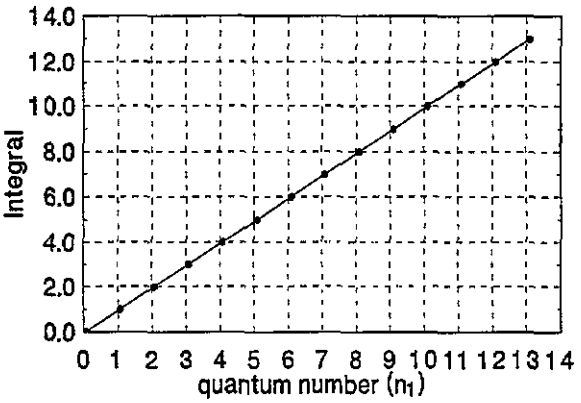

Figure 5. Plot of the values of the right-hand-side of (3.18*a*) for $N = 56$ computed numerically versus the possible integer values of the quantum number n_1.

$$u^{(h)} = \frac{-e}{\sqrt{2}z^{(h)}} \tag{3.18b}$$

$$z^3 - \frac{z}{2} - \frac{e}{4\sqrt{2}} = 0. \tag{3.18c}$$

Notice that the condition $e^2 = \frac{16}{27}$ corresponds to (3.11) and that $z^{(1)}$ and $z^{(2)}$ are the two positive solutions of the cubic equation for z.

We can now compare with the exact solutions of the quantum Hamiltonian. This can be accomplished upon plugging the exact eigenvalues E_0 and E_{int} obtained in section 2 into (3.18*a*), identifying approximately E_0 and E_{int} with $E_{0,c}$ and $E_{\text{int},c}$ for suitably large N (say, $N \geqslant 12$) (note, however, that in the visible range this corresponds to a typical intensity of 3×10^{-14} W cm^{-2}) and evaluating numerically the integral in (3.18*a*) in order to see whether it equals an integer, namely, the quantum number n_1. In figure 5 we can see this fitting for $N = 56$. One may then conclude that the quasiclassical representations are consistent with the results obtained for the exact quantum eigenvalues provided that $N \geqslant 12$ with an error not greater than 2%.

An interesting consequence is then that (3.18*a*) yields the eigenvalue E_{int} in terms of $E_0 = \hbar\omega N$ and n_1 in the quasiclassical limit.

A qualitative study of the left-hand side of (3.18*a*) for $j = 2$, using the values of $p_{1,c}(\sigma, \rho)$, $p_{2,c}(\sigma, \rho)$ seems to indicate that the former is different from zero, as it should be. As yet, we have not found any special curve Γ_2 such that it simplifies to any previously known (elementary or non-elementary) integral. Anyway, it is less relevant in practice than the integral for $j = 1$, which already yielded the relationship among E_0, E_{int} and n_1.

Finally, we shall provide some approximate formulae for the wavefunctions in this quasiclassical regime. We anticipate that our results have a rather limited scope.

In fact, while reliable one-dimensional quasiclassical wavefunctions are well known in all regions, elaborate formalisms yielding practical wavefunctions in more than one dimension appear to be lacking (leaving aside some mathematical studies which seem to be rather difficult to apply [25–28]).

The univaluedness and the connection formulae for the quasiclassical wavefunction in one dimension have been well understood and controlled. The univaluedness amounts to the quasiclassical quantization rules, which yield the eigenvalues in this approximation. Unfortunately, for systems in two or more dimensions, like the two-oscillator model treated in the present work, the situation is far more complicated and, hence, the available techniques have a more limited scope. In this case a crucial matter, namely, the generalization of the connection formulae, still appears to stand as an open problem.

Let the wavefunction $\psi(x_1, x_2)$ be a common eigenfunction of both operators H_0 and $H_{\rm int}$

$$H_0\psi = E_0\psi \qquad H_{\rm int}\psi = E_{\rm int}\psi\,. \tag{3.19}$$

In what follows, let A denote a given point on any of the curves $C_+ = 0$ or $C_- = 0$. Also, let $X = (x_1, x_2)$ be a generic point in the sheet (σ, ρ) inside $R_+(\sigma, \rho)$, and τ_i a suitable open curve which starts at A and ends at X and lies entirely inside $R_+(\sigma, \rho)$ in the (σ, ρ) sheet.

In a rather direct analogy with the well known WBK solution in one spatial dimension, we can write the following approximate formula for ψ inside $R_+(\sigma, \rho)$:

$$\psi(x_1, x_2) \approx \sqrt{\wp_i(x_1, x_2)}\exp\left\{\frac{\mathrm{i}}{\hbar}\int_A^X \left[p_{1,c}(\sigma, \rho)\,\mathrm{d}x_1 + p_{2,c}(\sigma, \rho)\,\mathrm{d}x_2\right]\right\} \tag{3.20}$$

where $\wp_i(x_1, x_2) = \wp_i$ is a real non-negative function.

In order to characterize $\wp_i$ let us look for the solutions of (3.19) in the form

$$\sqrt{\wp_i(x_1, x_2)}\exp\left\{\frac{\mathrm{i}}{\hbar}S_c(x_1, x_2)\right\} \tag{3.21}$$

where S_c is real and remains finite as $\hbar \to 0$. After replacing (3.21) in (3.19), separating real and imaginary parts and letting $\hbar \to 0$, one finds that $p_{1,c} \equiv \partial S_c/\partial x_1$ and $p_{2,c} \equiv \partial S_c/\partial x_2$ satisfy (3.5). With the same substitutions, the right-hand sides of (3.6) allow us to write

$$S_c = \int_A^X \left[p_{1,c}(\sigma, \rho)\,\mathrm{d}x_1 + p_{2,c}(\sigma, \rho)\,\mathrm{d}x_2\right] \tag{3.22}$$

the integral being performed along τ_i. The above separation between real and imaginary parts also yields the following system that characterizes $\wp_i(x_1, x_2)$:

$$\frac{\partial}{\partial x_1}\left(\wp_i\frac{\partial S_c}{\partial x_1}\right) + \frac{\partial}{\partial x_2}\left(\wp_i\frac{\partial S_c}{\partial x_2}\right) = 0 \tag{3.23a}$$

$$\frac{\sqrt{2\omega}x_2}{\omega}\frac{\partial}{\partial x_1}\left(\wp_i\frac{\partial S_c}{\partial x_1}\right) - \frac{\wp_i}{\sqrt{2\omega}}\frac{\partial S_c}{\partial x_2} - \frac{x_1}{\sqrt{2\omega}}\left[\frac{\partial}{\partial x_1}\left(\wp_i\frac{\partial S_c}{\partial x_2}\right) + \frac{\partial}{\partial x_2}\left(\wp_i\frac{\partial S_c}{\partial x_1}\right)\right] = 0\,. \tag{3.23b}$$

Notice that (3.23a) appears to be a continuity equation in (x_1, x_2)-space. $\wp_i$ could eventually be interpreted as some sort of probability density (but beware that x_1 and x_2 do not represent position for photons in ordinary space).

The solutions of (3.19) when X lies outside both R_+ and R_- (in any sheet) can also be written immediately, in a formal analogy with (3.20). Such a solution turns out to be rather difficult to analyse, depending on the signs of the imaginary parts of both $p_{1,c}$ and $p_{2,c}$. The possibility of tunnelling effects between R_+ and R_- (in each sheet), which are allowed in principle, adds further difficulties. A detailed analysis of how the wavefunction inside $R_+(\sigma, \rho)$ given in (3.20) would be connected to the quasiclassical solution outside $R_+(\sigma, \rho)$ definitely lies outside the realm of the present paper. Actually it would call for elaborate formalisms yielding WBK solutions and their connection formulae in more than one dimension, which appear to be lacking at present, as commented above.

To finish, we notice that (3.20) suffices to derive the quantization rule (3.13), which provides a clear check of consistency for the former. In fact, by choosing a suitable closed curve in the four-sheeted covering space and by imposing single-valuedness to (3.20) and by following Keller's argument, one arrives at (3.13).

4. Conclusions

We have examined the asymptotic behaviour of second-harmonic generation. The quantum dynamics of the model has been studied resorting to the technique of tridiagonal matrices. The important point is the largest possible eigenvalue for the interaction Hamiltonian scales as $N^{3/2}$, where N is the total photon number.

In the quasiclassical regime, we have derived two general equations yielding the spectrum of the problem. In this context, second-harmonic generation is a highly non-trivial application of the quasiclassical quantization rules, since the covering space of the problem shows an intriguing topological structure. These equations are fairly consistent for suitably large quantum numbers with the exact quantum results. We have also provided an approximate analytic expression for the wavefunction of the system.

Acknowledgments

We are grateful to Professors Ryszard Tanaś, Richard Barakat and Gabriel Alvarez for several interesting and fruitful discussions. Previous results of Professor S Dehesa on orthogonal polynomials were also useful. The partial financial support of CICYT (project AEN90-0034) is acknowledged by two of us (RFA-E and AGN).

References

[1] Bloembergen N 1972 *Nonlinear Optics* (New York: McGraw-Hill)
[2] Shen Y R 1985 *The Principles of Nonlinear Optics* (New York: Wiley)
[3] Jurco B 1989 *J. Math. Phys.* **30** 1739
[4] Carusotto S 1989 *Phys. Rev.* A **40** 1848
[5] Tucker J and Walls D F 1969 *Phys. Rev.* **178** 2036
[6] Persico F and Vetri G 1975 *Phys. Rev.* A **12** 1513
[7] Bonifacio R and Preparata G 1970 *Phys. Rev.* A **2** 336
[8] Kumar S and Mehta C L 1980 *Phys. Rev.* A **21** 1573
[9] Walls D F and Barakat R 1970 *Phys. Rev.* A **1** 446
[10] Walls D F and Tindle C 1971 *Nuovo Cimento Lett.* **2** 915; 1972 *J. Phys. A: Math. Gen.* **8** 534
[11] Mostovski J and Rzążewski K 1978 *Phys. Lett.* **66A** 275
[12] Kozierovski M and Tanaś R 1977 *Opt. Commun.* **21** 229
[13] Mandel L 1982 *Opt. Commun.* **42** 437
[14] Wu L, Kimble H J, Hall J L and Wu H 1986 *Phys. Rev. Lett.* **57** 2520
[15] Drobný G, Jex I and Buzek V 1993 *Phys. Rev.* A **48** 569
Drobný G and Jex I 1992 *Phys. Rev.* A **46** 499
[16] Nikitin S P and Masalov A V 1991 *Quantum Opt.* **3** 105
[17] Gantsog Ts and Tanaś R 1991 *Quantum Opt.* **1** 33
[18] Miranowicz A, Tanaś R and Kielich S 1990 *Quantum Opt.* **2** 253
[19] Tanaś R, Gantsog Ts and Zawodny R 1991 *Quantum Opt.* **3** 221
[20] Yoo H I and Eberly J H 1985 *Phys. Rep.* **118** 239
[21] Loudon R and Knight P L 1987 *J. Mod. Opt.* **34** 709
[22] Einstein A 1917 *Verhandl. dent. Physik Ges.*
[23] Brillouin L 1926 *J. Phys. Radium* **7** 353
[24] Keller J B 1958 *Ann. Phys., NY* **4** 180
[25] Berry M V and Mount K E 1972 *Rep. Prog. Phys.* **35** 315
[26] Maslov V P 1972 *Theorie des Perturbations et Methodes Asymptotiques* (Paris: Dunod) ch 2
[27] Schulman L S 1981 *Techniques and Applications of Path Integration* (New York: Wiley) ch 13–8
[28] Meyer R E 1991 Exponential asymptotics for partial differential equations *Asymptotics Beyond All Orders* ed H Segur *et al* (New York: Plenum)